Supplementary information

Direct optical fiber monitor on stress evolution of the sulfur-based cathodes for lithium-sulfur batteries†

Ziyun Miao,‡[a] Yanpeng Li,‡[b] Xiangpeng Xiao,[b] Qizhen Sun,*[b] Bin He,[a] Xue Chen,[a] Yaqi Liao,[a] Yi Zhang,[a] Lixia Yuan,[a] Zhijun Yan,[b] Zhen Li*[a] and Yunhui Huang*[a]

[a] State Key Laboratory of Material Processing and Die & Mould Technology, School of Materials Science and Engineering, Huazhong University of Science and Technology, Wuhan, 430074, China.

[b] National Engineering Laboratory for Next Generation Internet Access System, School of Optical and Electronic Information, Huazhong University of Science and Technology, Wuhan, 430074, China.

‡ These authors contributed equally to this work.

*Corresponding authors: qzsun@mail.hust.edu.cn (Q.S.), li_zhen@hust.edu.cn (Z.L.), huangyh@hust.edu.cn (Y.H.)

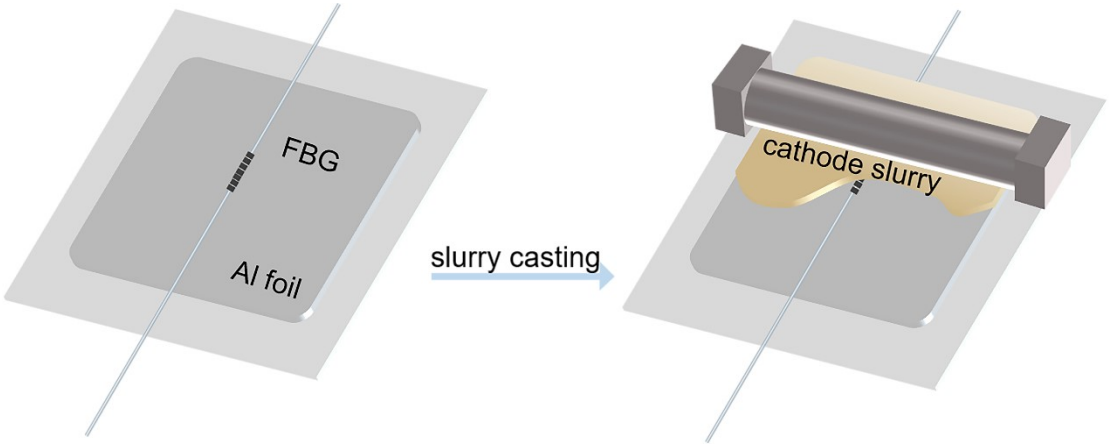

Fig. S1 The schematic illustration of the process of embedding FBG inside the cathode.

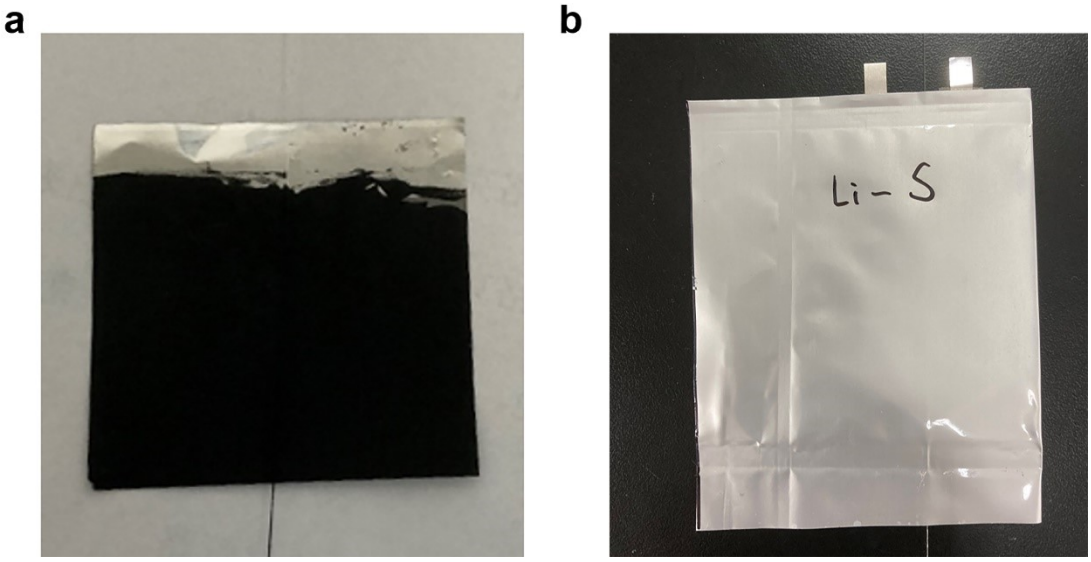

Fig. S2 Digital photos of the electrode and cell. (a) is for the sulfur cathode embedded with FBG and (b) is for the pouch cell appearance with a FBG embedded inside the cathode.

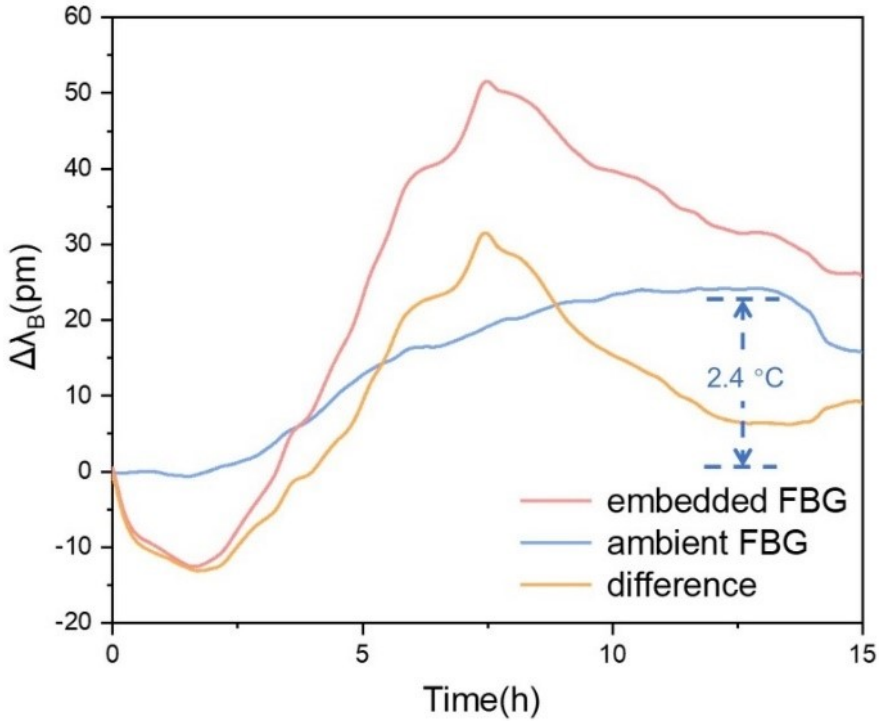

Fig. S3 The wavelength shifts of both the internal and ambient FBG during one discharge-charge cycle in solid-liquid-solid mechanism. It can be seen that the maximum wavelength shift of the ambient FBG is ~24 pm, corresponding to the ambient temperature change of ~2.4 °C. (The temperature sensitivity of bare FBG is about 10 pm/°C, which can be referred to reference 28). The raw data measured by the embedded FBG could not totally reflect the law of stress change, for the external change would cover some subtle internal signals. By subtracting the temperature shift, the processed data are much closer to the real situation of the stress change. The results further prove that our differential processing method is effective, even in an ordinary environment where the temperature control is not particularly strict.

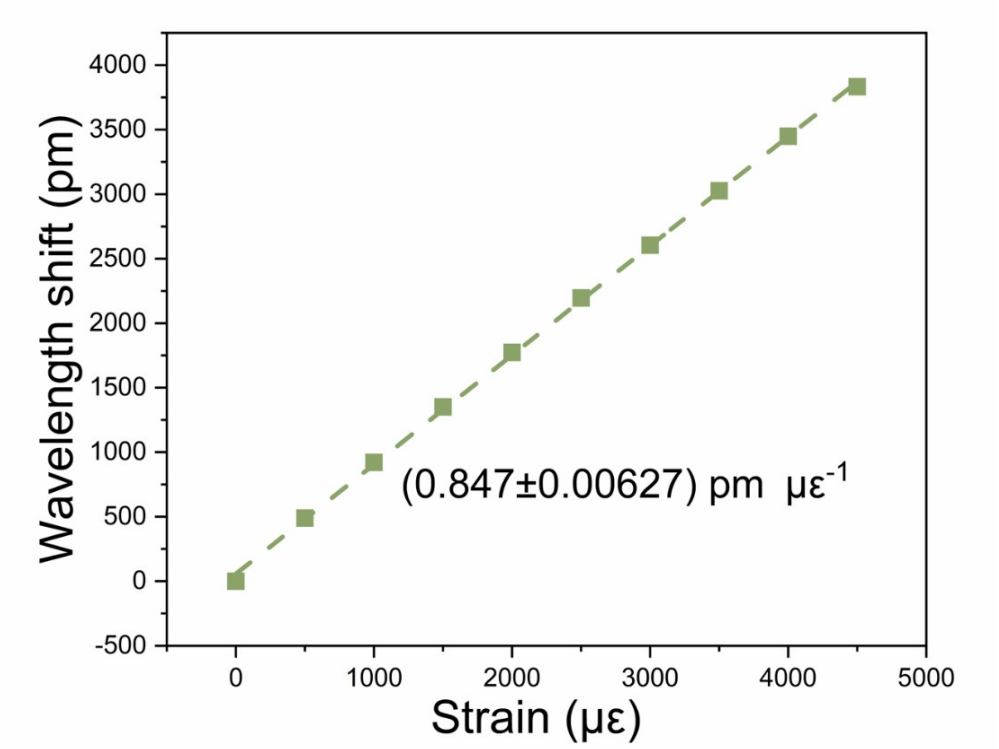

Fig. S4 The wavelength responses of a FBG to strain. The points are linearly fitted by the green dashed line. The linear relationship with the root mean squared error of the slope is given.

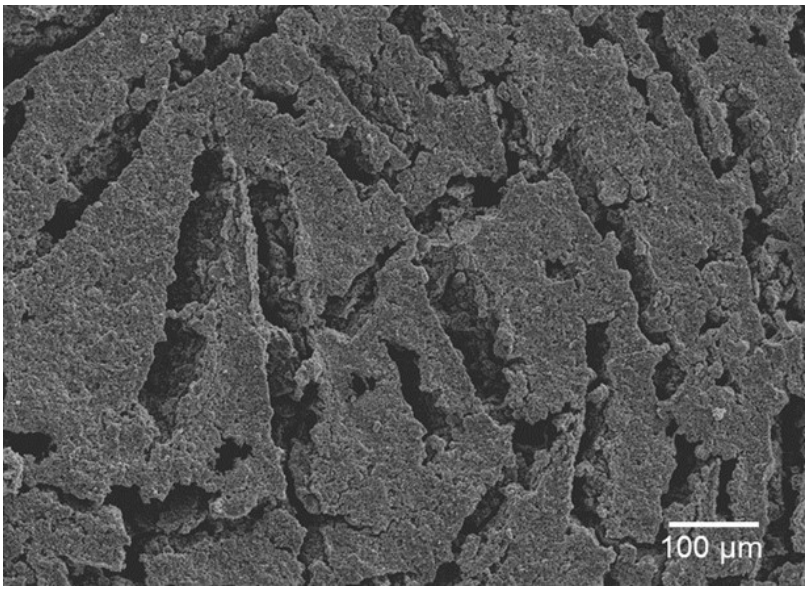

Fig. S5 The SEM image of KB/S cathode surface after the cell is charged.

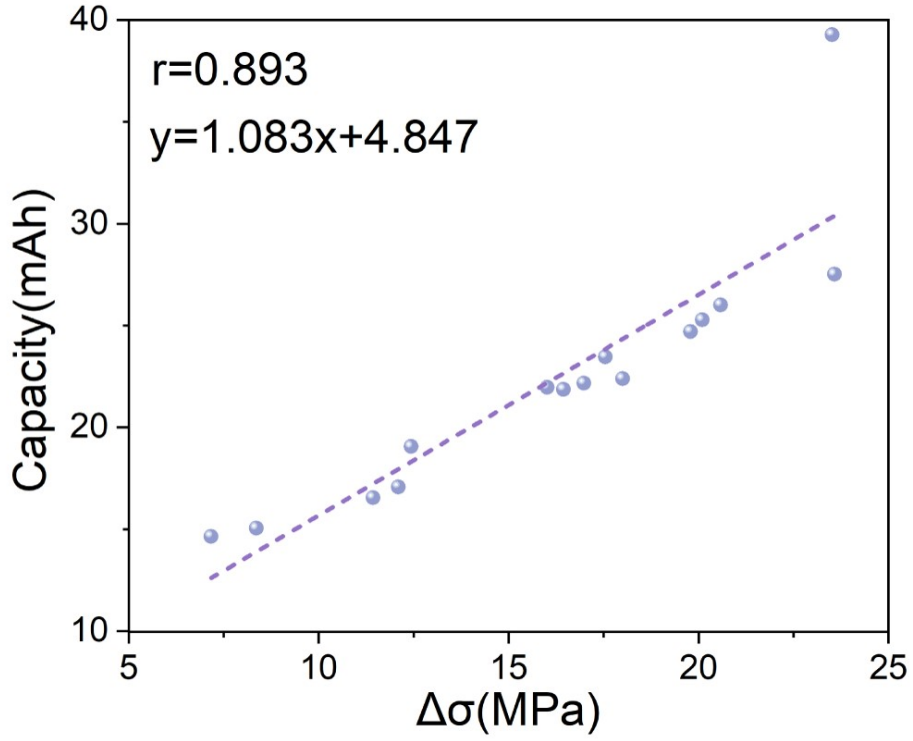

Fig. S6 The relationship between the discharge capacity and stress variation in the solid-solid conversion. The points are linearly fitted by the purple dashed line with correlation coefficient of 0.893.

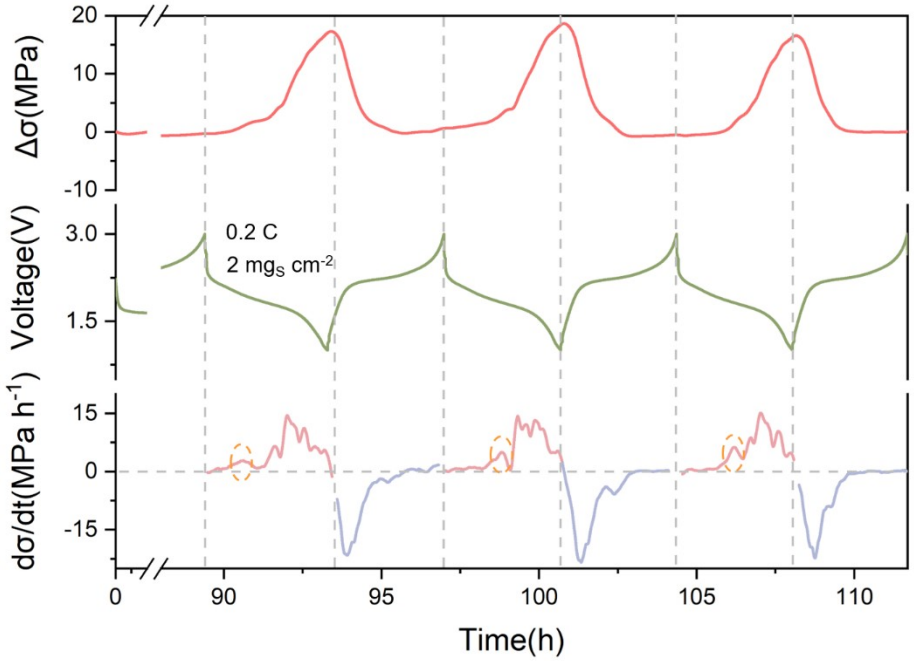

Fig. S7 The stress variation curve and corresponding charge-discharge curve under solid-solid mechanism. The stress curve is in the top panel, the corresponding galvanostatic discharge-charge curve (0.2 C) is in the middle panel and the differential curve of stress is in the bottom panel. The small peak on the d^{σ}/dt curve during discharge can still be observed (circled in the orange dashed line).

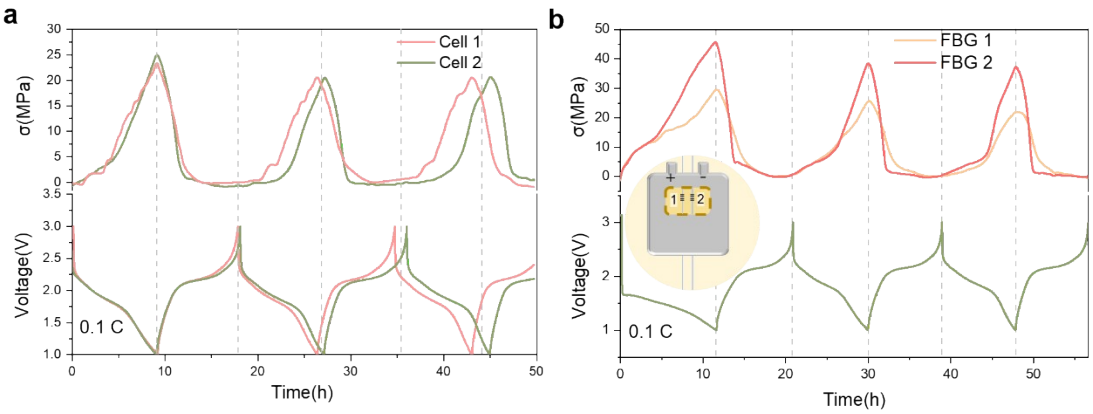

Fig. S8 (a) The stress and voltage curves of two cells with a FBG sensor embedded separately. (b) The stress and voltage curves of one cell with two FBG sensors embedded. The positions of the sensors are marked with a zoom-out schematic figure. The two FBGs are embedded between the two tabs, where FBG 1 is near the cathode tab and FBG 2 is near the anode tab.

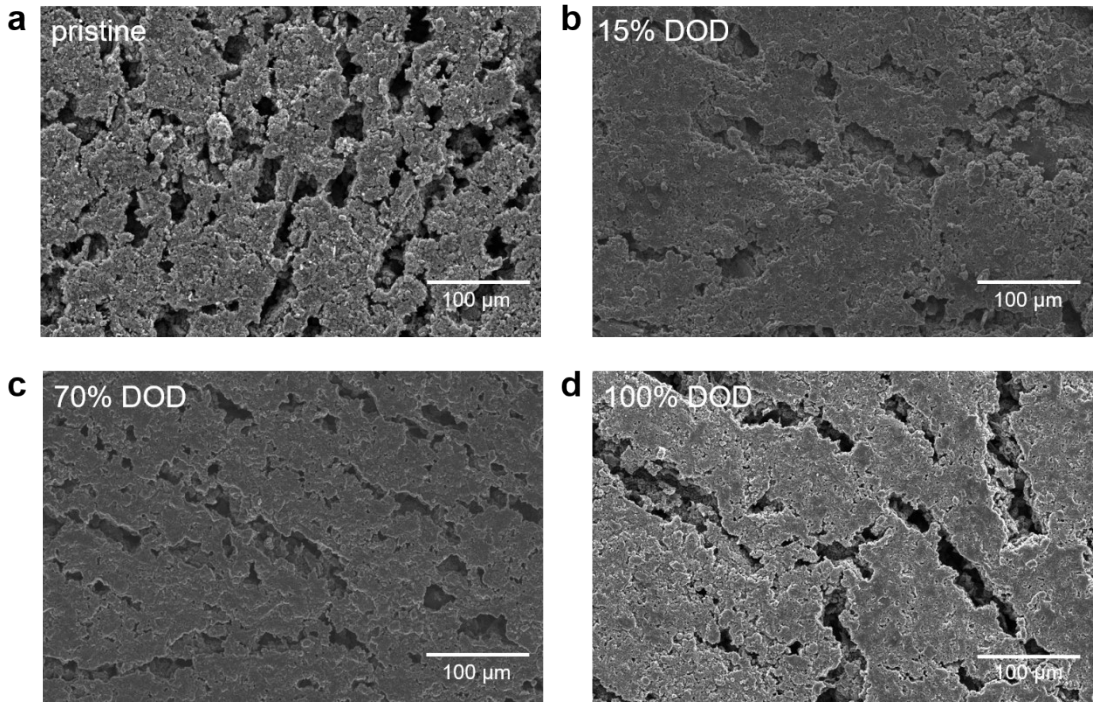

Fig. S9 SEM images of KB/S electrode surfaces which are (a)pristine, (b)15%, (c) 70% and (d) 100% DOD. The sulfur loading of the electrode is controlled among 3.5-4 mg_S cm^{-2}.

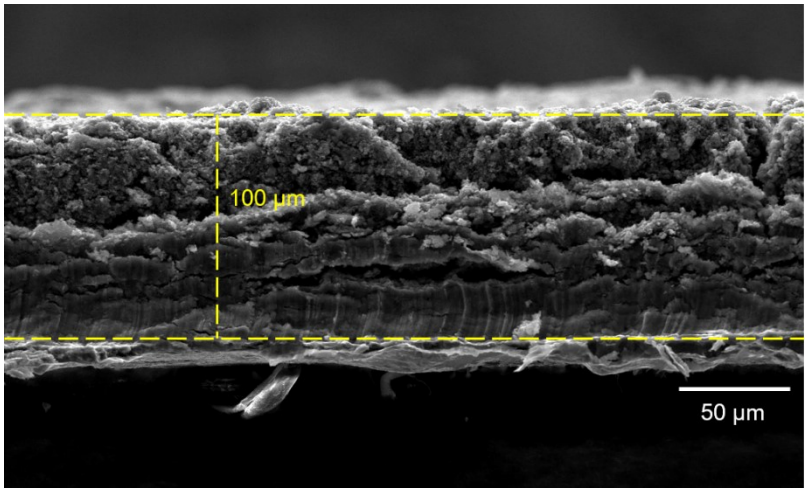

Fig. S10 The cross-sectional SEM image of the pristine PANS electrode before any electrochemical measurement.

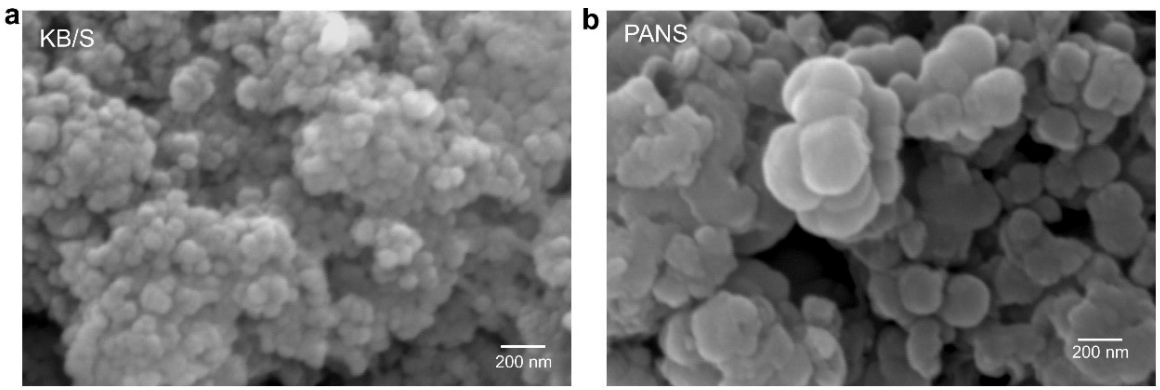

Fig. S11 SEM images of particles in (a) KB/S cathode and (b) PANS cathode.

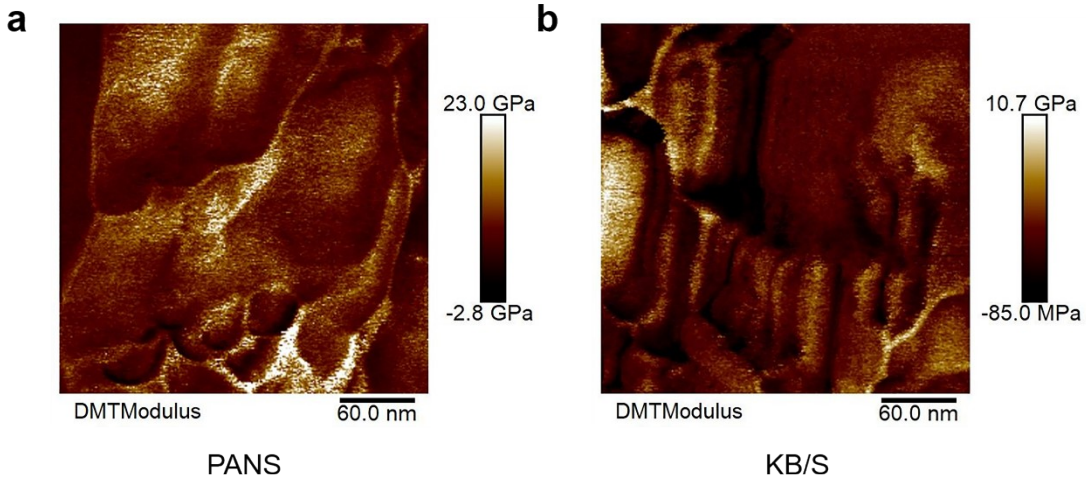

Fig. S12 Two-dimensional images of the elastic modulus distribution characterized by atomic force microscopy (AFM). (a) is based on a pristine PANS electrode and (b) is based on a pristine KB/S electrode.

Table S1 List of parameters involved in porosity calculations.

Materials		S	C	PAN	Binder	Total
Density (g cm^{-3})		2.07	2.02	1.184	1.76	
Weight percentage (%)	KB/S	63	27		10	100
	PANS	33.2	10	46.8	10	100
Mass (mg)	KB/S	2.5	1.07		0.4	3.97
	PANS	1	0.3	1.41	0.3	3.01
Dense volume (mm^3)	KB/S	1.21	0.53		0.22	1.96
	PANS	0.48	0.15	1.19	0.17	1.99